Many-body interactions and correlations in coarse-grained descriptions of polymer solutions

P. G. Bolhuis,* A. A. Louis,† and J. P. Hansen
Department of Chemistry, Lensfield Road, Cambridge CB2 1EW, United Kingdom
(Received 8 March 2001; published 23 July 2001)

We calculate the two-, three-, four-, and five-body (state-independent) effective potentials between the centers of mass (c.m.'s) of self-avoiding walk polymers by Monte Carlo simulations. For full overlap, these coarse-grained n-body interactions oscillate in sign as $(-1)^n$, and decrease in absolute magnitude with increasing n. We find semiquantitative agreement with a scaling theory, and use this to discuss how the coarse-grained free energy converges when expanded to arbitrary order in the many-body potentials. We also derive effective *density dependent* two-body potentials that exactly reproduce the pair-correlations between the c.m. of the self avoiding walk polymers. The density dependence of these pair potentials can be largely understood from the effects of the *density independent* three-body potential. Triplet correlations between the c.m. of the polymers are surprisingly well, but not exactly, described by our coarse-grained effective pair potential picture. In fact, we demonstrate that a pair potential cannot simultaneously reproduce the two- and three-body correlations in a system with many-body interactions. However, the deviations that do occur in our system are very small, and can be explained by the direct influence of three-body potentials.

DOI: 10.1103/PhysRevE.64.021801 PACS number(s): 61.25.Hq, 61.20.Gy

I. INTRODUCTION

An efficient statistical description of condensed matter systems and materials almost invariably involves some degree of coarse graining, whereby a large fraction of the initial microscopic degrees of freedom are traced out, leaving a much reduced space of variables associated with the composite entities or pseudoparticles. The latter are then coupled via effective interactions that result from the partial averaging over the initial microscopic degrees of freedom. The reduction of the initial multicomponent system to a coarse-grained system with a substantially smaller set of composite particles implies that the resulting effective interactions may involve three-body and higher-order contributions, even if the original multicomponent system involved only pairwise additive forces, like Coulombic interactions. Alternatively, one may wish to retain the simplicity of pairwise additivity of the effective interactions, but the price to pay is that such effective pair potentials are then state dependent, e.g., are functions of the temperature and/or density. The reason for this is that the effective interaction energy is a free energy associated with the averaged-out degrees of freedom, which generally has an entropic component.

There are many examples of the coarse-graining procedure that has just been outlined. In molecular systems the forces between nuclei result from gradients of the electronic ground state energy surface, which depends parametrically on the nuclear coordinates, and adjusts adiabatically to the slow motion of the latter within the Born-Oppenheimer approximation. This scenario is mimicked, at least at the level of valence electrons, in *ab initio* molecular dynamics simulations pioneered by Car and Parrinello [1]. However, in situations where no strong covalent or hydrogen bonding is present, the more common route is to represent the total ground state electronic energy surface by a sum of one-body, two-body, and higher order terms. The one-body contribution is the sum of the ground state energies associated with individual, isolated chemical entities (atoms, ions, or molecules). The two-body term is made up of the sum of pair potentials acting between molecules and higher-order terms correspond to isolated clusters of three or more molecules. The sum of ground state energies of individual molecules does not contribute to the forces between them, and can hence be ignored in the description of collective equilibrium or transport processes that do not involve chemical reactions. In the simplest case of rare-gas atoms, the pairwise interactions would include overlap repulsion at short range and dispersion forces at long range, while triplet interactions would include, among others, the Axilrod-Teller triple dipole dispersion potential [2], which contributes very significantly to the thermodynamic and transport properties of the heavier rare gases in their condensed states [3,4]. The effect of the higher-order interactions can be approximately incorporated into an effective pair potential, which differs from the bare pair potential, valid for an isolated pair of molecules, and becomes density dependent [5,6].

Similarly, in metals an effective interaction between ions may be determined by tracing out the conduction electrons, using perturbation theory or response theory [7,8]. Treating the ion-electron coupling to lowest order (linear response) leads to a structure-independent volume term and to a pairwise screened effective potential between ''dressed'' ions or pseudo-atoms, which both depend on the macroscopic conduction electron density. The two-body level is generally sufficient for alkali and other simple metals, in part because of a quantum interference effect that strongly decreases the magnitude of the higher-order response terms [9]. For multivalent and transition metals many-body effective interactions can no longer be neglected [8], and a full *ab initio* treatment may be necessary [10].

Coarse-graining becomes crucial in the highly asymmetric systems of soft matter, involving macromolecules or colloi-

*Email address: bolhuis@its.chem.uva.nl
†Email address: ardlouis@theor.ch.cam.ac.uk

dal particles, as well as molecular scale entities, like solvent molecules or ions. The latter are traced out to derive effective interactions between the electric double-layers associated with charged surfaces (colloids, membranes, etc.) [11]. The microscopic ions play a role similar to valence electrons in metals, but with the important difference that quantum degeneracy effects are absent, and that finite temperature entropic effects control the width of the electric double layers, with a resulting density and temperature dependence of the effective interactions between the mesoscopic colloidal particles. A good example of a such a pair potential is provided by the classic Derjaguin-Landau-Verwey-Overbeek effective pair potential between spherical charged colloidal particles [11]. Three-body interactions can be derived in similar fashion [12]. However, the averaging over the microion degrees of freedom also leads to a structure-independent, but state-dependent volume term, part of which is associated with the self-energy of individual double layers, and which is reminiscent of the volume term in metals [13,14]; this term has a profound effect on the phase diagram of charge-stabilized colloids [14,15].

Another important class of effective interactions of entropic origin, which follow from averaging over the configurations of nonadsorbing polymers and small colloidal particles, are the depletion forces that have received much renewed interest in recent years [16,17]. Depletion pair potentials depend strongly on the concentration of the depletant; recent attempts have been made to compute the three-body interactions from simulations or density functional theory [18]. Volume terms arising from the depletion potential picture may have an important effect on the osmotic equation of state, but they are not expected to influence the phase behavior in these uncharged systems [16].

The present paper is concerned with a coarse-grained description of dilute and semidilute solutions of polymers in good solvent. Whereas tracing out the microscopic ions in a charged colloidal suspension has many analogies with the liquid metal problem, the coarse graining of neutral polymers, achieved by integrating out the internal monomeric degrees of freedom, resembles more closely the case of effective potentials between neutral atoms and molecules, obtained by tracing out the internal electronic degrees of freedom. The basic idea explored here, which goes back to Flory and Krigbaum [19], is to represent a set of polymers, each made up of L monomers or segments, as single particles, interacting with each other through an effective interaction between their centers of mass (c.m.'s). The important point, realized by Grosberg *et al.* [20], is that the effective pair interaction remains finite, even for infinitely long polymers. Monte Carlo simulations [21] and renormalization group calculations [22] show that for two isolated nonintersecting polymer coils, the effective potential between their c.m.'s is of order $2k_BT$ in the scaling limit, i.e., for L going to infinity, while the range of the interaction is of the order of the radius of gyration R_g of the polymers. Recently we have extended this investigation by simulating large systems of self-avoiding walk (SAW) polymers at *finite* concentration [23,24]. The resulting c.m. pair distribution function $g(r)$ was then inverted to yield a concentration-dependent effective pair potential $v(r;\rho)$, where ρ is the number of polymer coils per unit volume. Although $v(r;\rho)$ was not found to change dramatically with ρ, the ρ dependence of v is very significant for the accurate determination of the osmotic properties of dilute and semidilute polymer solutions.

In this paper we adopt a somewhat different point of view, by determining state-independent effective pair, triplet, quadruplet, and quintuplet interactions; these many-body interactions are determined by successively considering clusters of 2, 3, 4, and 5 SAW polymer chains, determining the corresponding n-body distribution functions, from which an effective n-body potential is derived. Triplet interactions between the cores of star polymers have recently been determined in a similar way [25]. The next step taken in this paper is to relate the low-density (state-independent) pair and triplet interactions to the density-dependent effective interactions determined in our earlier work [23,24]. A final section will be devoted to an analysis of three-body correlations as measured by bond-angle distributions and deviations from the Kirkwood superposition approximation [26]. The convergence of the series of n-body interactions is assessed on the basis of scaling arguments in the appendixes.

II. SIMULATION MODELS AND METHODS

Many properties of polymers in a good solvent are well described by models that ignore all microscopic details of the intermolecular interactions, except their excluded volume. For that reason polymers are often modeled as self-avoiding walks on a lattice [27–29], a model lending itself well to efficient computer simulations. We consider the situation of N athermal SAW chains of length L on a simple cubic lattice of M sites. The bead or segment concentration is given by $c=NL/M$, while the polymer chain concentration is given by $\rho=N/M$. The polymers are characterized by their radius of gyration R_g which, for an isolated polymer, scales as $R_g \sim L^{\nu}$, where $\nu \approx 0.59$ is the Flory exponent [27–29]. We also define an overlap concentration $\rho^* = 1/\frac{4}{3}\pi R_g^3$ at which there is on average one polymer per sphere of radius R_g. Solutions with $\rho/\rho^* < 1$ are called dilute, while solutions with $\rho/\rho^* > 1$ and $c \ll 1$ are called semidilute. When the monomer density c becomes appreciable, the solution moves from the semidilute to the melt regime. In this paper we will focus on densities $\rho/\rho^* \lesssim 2$, i.e., the dilute regime and the beginning of the semidilute regime.

When modeling the semidilute regime, it is important to take sufficiently long polymer chains. The first reason is that for studying the semidilute regime one needs a large polymer density ρ together with a low monomer density c. We found earlier that the monomer density c^* at the overlap concentration ρ^* scales roughly like [24] $c^* \approx 4L^{-0.8}$ for SAW polymers on a simple cubic lattice. Throughout this paper we use polymers of length $L=500$ for which $c \approx 0.05$ at $\rho/\rho^* = 2$, so that we are still clearly in the semidilute regime. In contrast, for $L=100$ the monomer density is $c \approx 0.2$ at $\rho/\rho^* = 2$, suggesting that a meaningful semidilute regime does not exist for such short polymers.

The second reason for using long polymer chains is that we want to study properties—particularly the effective po-

tentials between polymer chains—in the scaling regime, where all length dependence is completely captured by R_g. In a previous paper [24] we established that two properties of the effective potential relevant to thermodynamics, namely, the second-virial coefficient B_2 between two polymers and the effective pair potential between c.m.'s, multiplied by the square of the c.m. distance $r^2v(r)$ are very close to the scaling limit for $L=500$ polymers, the length we will use in this paper.

Simulations were done with the Monte Carlo pivot algorithm [21,30] combined with simple translational moves. For concentrations $\rho>\rho^*$ we also use configurational bias Monte Carlo (MC) algorithms [31,32]. For $L=500$ polymers we find that the radius of gyration of an isolated coil is $R_g=16.50\pm0.03$. We used a simulation box of size $M=(240)^3$, and varied the number of polymers from $N=2$ for the two-body calculations to $N=6400$, which corresponds to $\rho/\rho^*=8.9$.

Since we are dealing with athermal chains consisting of monomers interacting only via hard-core repulsion, we set the reciprocal temperature $\beta=1/k_BT=1$ throughout this paper.

III. DENSITY INDEPENDENT MANY-BODY INTERACTIONS

A. Expanding the coarse-grained free energy in a series of many-body interactions

Following the discussion in [33], the Helmholtz free energy $\mathcal{F}$ of a set of N polymers of length L with their c.m.'s distributed according to the set of coordinates $\{\mathbf{r}_i\}$, in a volume V, can be written as the following expansion:

$$\mathcal{F}(N,V,\{\mathbf{r}_i\})=\mathcal{F}^{(0)}(N,V)+\sum_{i_1<i_2}^{N} w^{(2)}(\mathbf{r}_{i_1},\mathbf{r}_{i_2}) + \sum_{i_1<i_2<i_3}^{N} w^{(3)}(\mathbf{r}_{i_1},\mathbf{r}_{i_2},\mathbf{r}_{i_3}) + \cdots w^{(N)}(\mathbf{r}_{i_1},\mathbf{r}_{i_2},\ldots\mathbf{r}_{i_N}). \quad (1)$$

In the scaling limit, each term in the series is independent of L as long as the n-tuple c.m. coordinates $\{\mathbf{r}_{i_1},\mathbf{r}_{i_2}\cdots\mathbf{r}_{i_n}\}$ are expressed in units of R_g, the radius of gyration at zero density. Note that this coarse-grained free energy includes an implicit statistical average over all the monomeric degrees of freedom for a fixed configuration $\{\mathbf{r}_i\}$ of the c.m. The full free energy of the underlying polymer system can be calculated as follows:

$$F(N,V)=-\ln\int\cdots\int dr_i\ldots dr_N \exp[-\mathcal{F}(N,V,\{\mathbf{r}_i\})], \quad (2)$$

so that Eq. (1) can be viewed as an expansion of the effective interaction between the c.m. in terms of (entropic) many-body interactions. $\mathcal{F}^{(0)}(N,V)$ is the so-called volume term, the contribution to the free energy that is independent of the configuration $\{\mathbf{r}_i\}$ [14]. Here it includes the free energy of a single isolated polymer, which is independent of the position of its c.m. in a homogeneous solution; translational invariance also implies that there is no one-body term in the expansion. Each subsequent term $w^{(n)}(\mathbf{r}_{i_1},\mathbf{r}_{i_2},\ldots,\mathbf{r}_{i_n})$ is defined as the free energy of n polymers with their c.m. positions at $\{\mathbf{r}_{i_1},\mathbf{r}_{i_2},\ldots,\mathbf{r}_{i_n}\}$ minus the contributions of all lower-order terms. In other words, it is the contribution to the free energy of n polymers that is not included in the sum of all lower-order terms. For instance, the two-body term $w^{(2)}(r_{ij})$ can be defined as the difference between the coarse-grained free energy $\mathcal{F}$ for two particles with their c.m. distance held at $r_{ij}=|\mathbf{r}_i-\mathbf{r}_j|$, and the free energy of the same two polymers when they are infinitely apart. Here we use the translational and rotational invariance of a homogeneous system to reduce the number of degrees of freedom. Similarly, the three-body term for a given triplet configuration $\{\mathbf{r}_i,\mathbf{r}_j,\mathbf{r}_k\}$ can be written in terms of only three variables (see Fig. 1) as

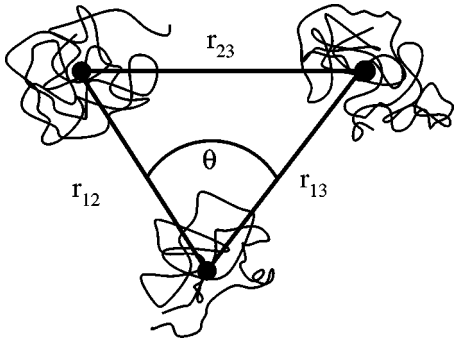

FIG. 1. The three variables $\{r_{12},r_{13},r_{23}\}$ that characterize a triplet configuration. The angle θ between the vectors $\mathbf{r}_{12}$ and $\mathbf{r}_{13}$ is related to the distance r_{23} by $r_{23}^2=r_{12}^2+r_{13}^2-2r_{12}r_{13}\cos\theta$.

$$w^{(3)}(r_{ij},r_{jk},r_{ki})=\mathcal{F}(N=3,V,r_{ij},r_{jk},r_{ki})-\mathcal{F}^{(0)}(N=3,V) - w^{(2)}(r_{ij})-w^{(2)}(r_{ik})-w^{(2)}(r_{jk}). \quad (3)$$

In other words, it is that part of the effective interaction between three polymers that cannot be described by volume and pair interaction terms alone. In principle, this procedure may be continued until, for a system with N polymers, the Nth term determines the total coarse-grained free energy. In practice, this approach is not feasible because the number of n-tuple coordinates increases rapidly with n, as does the complexity of each higher-order term, so that the series in Eq. (1) quickly becomes intractable. Instead, one hopes to show that the series converges fast enough that only a few low-order terms are needed to obtain a desired accuracy. We now turn to the derivation of these density-independent potentials for our system of SAW polymers.

B. Two-body interactions

There is a general relationship between the $\rho\to0$ limit of n-body correlation functions and the n-body potential [33]. For the two-body case this reduces to

$$\lim_{\rho\to0} g_2(r)=\exp[-w^{(2)}(r)], \quad (4)$$

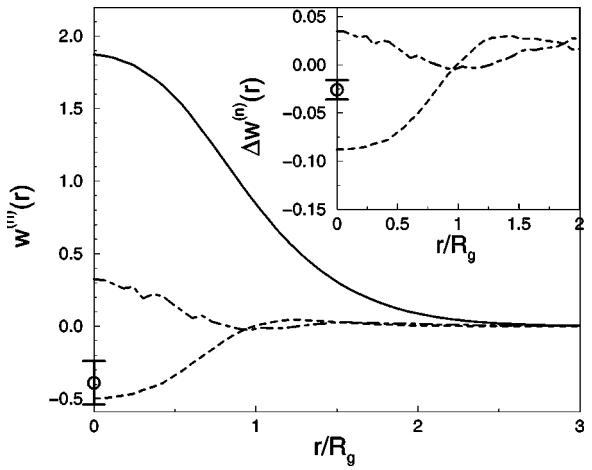

FIG. 2. Effective potentials $w^{(n)}(r)$ for $n=2$ (solid line), $n=3$ (dashed line), $n=4$ (dash-dotted line), and $n=5$ (symbol with error bar at $r=0$). Inset: relative potentials $\Delta w^{(n)}(r)$ for $n=3$ (dashed line), $n=4$ (dash-dotted line), and $n=5$ (symbol with error bar at $r=0$).

where $g_2(r)$ is the pair distribution function. Although this definition resembles that of the potential of mean force (PMF), usually defined as $w^{PMF}(r)=-\ln[g_2(r)]$ for any density, they are only equivalent in the limit of infinite dilution. Strictly speaking, the PMF is not a potential but simply a restatement of the pair correlations. Consider the simplest case, namely, a system with no higher-order ($n>2$) interactions. If one were to use a finite density PMF as a pair potential at that same finite density, the resulting pair correlations would not be those of the system used to derive the PMF. In contrast, the potential defined in Eq. (4) is the correct pair potential that would exactly reproduce the pair correlations of the original system.

In our simulations we calculate $w^{(2)}(r)$ from the logarithm of the overlap probability as a function of c.m. distance [cf. Eq. (4)]. Although the arguments above were made for a free energy in a continuous space, they easily carry over for the lattice model we simulate. In fact, the c.m. lives on a grid finer than the original SAW lattice polymers, so that our results are already closer to the continuum limit. The overlap probability is determined by sampling the configurations of two polymers infinitely apart with the pivot algorithm, and, after every 1000 pivot moves, searching for any monomer overlaps as a function of the c.m. distance. The effective potential calculated in this manner has a near Gaussian shape with a value at full overlap of $w^{(2)}(0)=1.88\pm0.01$ for our $L=500$ polymers, very close to the scaling limit estimate $w^{(2)}(0)=1.80\pm0.05$ [24], and a range of the order of R_g [23,24], as shown in Fig. 2. This picture agrees with earlier renormalization group [22] and simulation [21] studies. Note that in the scaling limit the potentials depend only on R_g, so that the free energy cost of completely overlapping the c.m. of two polymers is independent of their length L. That this free energy cost at complete overlap should depend weakly on polymer length follows from their fractal nature [19], but more sophisticated scaling theory arguments [20] are needed to prove that $w^{(2)}(0)\propto L^0$ [23,24].

C. Three-body interactions

Just as the two-body interactions follow from the low-density limit of the pair correlations, so also the three-body or triplet interactions between the c.m. of three polymers can be derived by taking the low-density limit of the three-body distribution function

$$g_3(\mathbf{r}_1,\mathbf{r}_2,\mathbf{r}_3)=\frac{1}{Z}\int\cdots\int e^{-\mathcal{F}(\{\mathbf{r}_i\})}d\mathbf{r}_4\cdots d\mathbf{r}_N, \qquad (5)$$

where $\mathcal{F}(\{\mathbf{r}_i\})$ is the coarse-grained free energy (1) and $Z=\exp[-F]$ is the configurational integral for the c.m. coordinates defined in Eq. (2). (Since the effective interactions already include an average over monomeric degrees of freedom, this configurational integral is equivalent to that of the full polymer system.) Taking the low-density limit for a homogeneous system gives

$$-w^{(3)}(r_{12},r_{23},r_{13})=\lim_{\rho\to0}\ln\left[\frac{g_3(r_{12},r_{23},r_{13})}{g_2(r_{12})g_2(r_{23})g_2(r_{13})}\right]. \qquad (6)$$

The $g_2(r)$ ensure that the contributions due to the pair interactions are subtracted from the triplet interaction [cf. Eq. (3)]. For our homogeneous system the three-body potential depends only on the three variables $\{r_{12},r_{23},r_{13}\}$ shown in Fig. 1. Even then, calculating the triplet interaction $w^{(3)}(r_{12},r_{23},r_{13})$ for every possible triplet arrangement is very cumbersome. We therefore confine ourselves to configurations that make up an equilateral triangle. Instead of three variables, the potential now depends only on the length r of each side of the triangle, simplifying the calculation of Eq. (6) to

$$w^{(3)}(r)=-\lim_{\rho\to0}[\ln g_3(r)-3w^{(2)}(r)], \qquad (7)$$

where we also used Eq. (4). We expect that for $r=0$, i.e., complete overlap, the three-body interaction will be strongest, while for large r the interaction should vanish.

We calculated $w^{(3)}(r)$ for three $L=500$ SAW polymers on a lattice. At this infinite dilution, $g_3(r)$ is simply the probability that three polymers in a configuration $\{r_{12},r_{23},r_{31}\}$ do not overlap. In the Monte Carlo simulation we integrate over the monomeric degrees of freedom by performing pivot moves. Once every 1000 MC steps we move the polymers into a triangular configuration and check for overlap. The results are plotted in Fig. 2. Since the total free energy increases with the number of polymers, a more relevant measure of the three-body interactions is the relative potential $\Delta w^{(3)}(r)=w^{(3)}(r)/3w^{(2)}(r)$ that denotes the strength of the three-body interaction relative to that of the two-body interactions. As shown in the inset of Fig. 2, the relative contribution of the three-body potential to the total free energy is quite small, only about 9% of the contribution from the pair potentials.

D. Four-body interactions

Next we turn to the four-body interactions. Again, even for a homogeneous phase, the total number of relevant coordinates makes the calculation of the full interaction prohibitively complex. To restrict the number of coordinates in our calculations we determine the four-body potential by placing the four polymer c.m.'s on a regular tetrahedron and determining the nonoverlap probability as a function of the length r of each side of the tetrahedron. The four-body potential is then defined as

$$w^{(4)}(r) = -\lim_{\rho\to 0} \ln[g_4(r)] - 4w^{(3)}(r) - 6w^{(2)}(r) \qquad (8)$$

since the tetrahedral configuration includes four equilateral triangles (three-body interactions) and six edges (two-body interactions). The full and relative four-body interaction, $\Delta w^{(4)}(r) = w^{(4)}(r)/[4w^{(3)}(r) + 6w^{(2)}(r)]$, are plotted in Fig. 2. Note that the four-body interaction is smaller in absolute magnitude and has the opposite sign to the three-body interaction. The relative contribution of the four-body interactions to the total free energy is less than 5% of the total potential, and also less than the relative three-body contribution.

E. Five-body interactions

Calculating the five-body interaction is even more complicated than the four-body interaction, and so we only evaluate it at full overlap—when all the c.m.'s coincide—where we expect its contribution to be largest. More generally, for any nth order term the interaction at full overlap is given by

$$w^{(n)}(0) = -\lim_{\rho\to 0}[\ln g_n(0)] - \sum_{m=2}^{m=n-1} \binom{n}{m} w^{(m)}(0), \qquad (9)$$

where $\lim_{\rho\to 0} g_n(0)$ is the normalized probability of full overlap of the c.m. of n polymers. As long as the particles are equidistant from each other, the same combinatorial expression holds for finite r. For the five-body term we find that $w^{(5)}(0) = -0.4 \pm 0.15$, while the relative contribution of the five-body terms is given by $w^{(5)}(0)/[5w^{(4)}(0) + 10w^{(3)}(0) + 10w^{(2)}(0)] = 0.026 \pm 0.01$. Again, the relative contribution of the five-body term to the free energy is smaller and of opposite sign to those of the four-body terms. Going beyond the five-body interaction, even at complete overlap becomes increasingly difficult. For example, for the five-body interaction, of the 10^8 overlap checks, each attempted after 1000 pivot moves, only about 30 resulted in nonoverlap. For the six-body interaction we estimate that 10^{11} MC overlap attempts would be needed. Another problem arises from finite monomer density. As more and more polymers overlap, the monomer density increases, so that in practice for a given polymer length L, only a finite number of multiple overlaps are possible. We found previously that the largest finite-size corrections to the scaling limit were at $r = 0$ for $w^{(2)}(0)$ [24]. The same probably holds for the higher-order interactions. However, our $L = 500$ calculations should still be very near the scaling limit.

IV. EFFECTIVE DENSITY-DEPENDENT PAIR INTERACTIONS

From the previous section we see that explicitly calculating the *density-independent* interactions $w^{(n)}(\mathbf{r}_{i_1}, \mathbf{r}_{i_2}, \ldots, \mathbf{r}_{i_N})$ becomes rapidly more complex with increasing order n. Calculating all higher-order terms is therefore impossible. In this section, we describe a way to include the average effect of all higher-order terms by extending the relationship between the pair interactions and the pair correlations to finite density ρ. This leads to a *density-dependent* effective pair interaction $v(r;\rho)$.

A. Inverting pair correlations to derive density-dependent pair potentials

Although for finite densities there is no known direct functional relationship of the type of Eq. (4), there is a theorem which states that for any given pair-correlation function $g_2(r)$ and density ρ, there exists (up to an additive constant) a unique pair potential $v(r;\rho)$ that exactly reproduces $g_2(r)$ at that density [34,35]. If the original $g_2(r)$ is generated by a system with only pair interactions, then $v(r;\rho) = w^{(2)}(r)$ will be independent of density. If there are any higher-order interactions in the original system that influence the structure, then this equivalence will only hold for $\lim_{\rho\to 0} v(r;\rho) = w^{(2)}(r)$. At finite densities $v(r;\rho)$ must change since the structure is no longer equal to the one generated by $w^{(2)}(r)$ alone. Therefore $v(r;\rho)$ must be density dependent.

In fact, this is what we found in two previous papers [23,24], where we used the hypernetted-chain (HNC) approximation from liquid state theory [36] to extract $v(r;\rho)$ from computer simulations of the $g_2(r)$'s between the c.m.'s of SAW polymers. For completeness, we show these effective pair interactions in Fig. 3. As expected, there is a clear density dependence. Without going into much detail about the inversion of $v(r;\rho)$ from $g_2(r)$, we do want to point out that the process can be very subtle. As illustrated in Fig. 4, the $g_2(r)$'s generated at $\rho = \rho^*$ by $v(r;\rho = 0)$ and $v(r;\rho = \rho^*)$ are very similar. Any technique to derive $v(r;\rho)$ from $g_2(r)$ must be significantly more accurate than the difference between the $g_2(r)$'s shown in the figure. The accuracy of the techniques we use has been discussed in Ref. [24], and will be analyzed in much more detail in another publication [37].

Any approximation that correctly reproduces the pair correlations will also predict the correct thermodynamics through the compressibility equation [36,38]. For our density-dependent $v(r;\rho)$ this is indeed the case, since we found good agreement between the equation of state (EOS) Π/ρ generated by the effective potentials in Fig. 3 and the EOS of the underlying SAW polymer solution. In contrast, the $v(r;\rho = 0)$ potential underestimates the EOS, and we find mean-field fluid behavior $\Pi/\rho \sim \rho$ at large ρ instead of the correct $\Pi/\rho \sim \rho^{1.3}$ scaling. So, even though the $\rho = 0$ potential results in pair correlations $g_2(r)$ that are similar to the true $g_2(r)$'s, the effective thermodynamics can differ signifi-

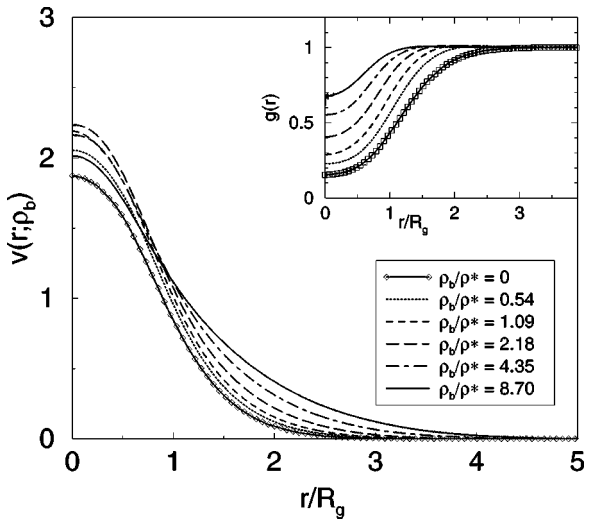

FIG. 3. The effective polymer pair potentials $v(r;\rho)$ derived at different densities from an HNC inversion of the c.m. pair distribution functions $g_2(r)$ of polymer coils depicted in the inset (from Ref. [24]) .

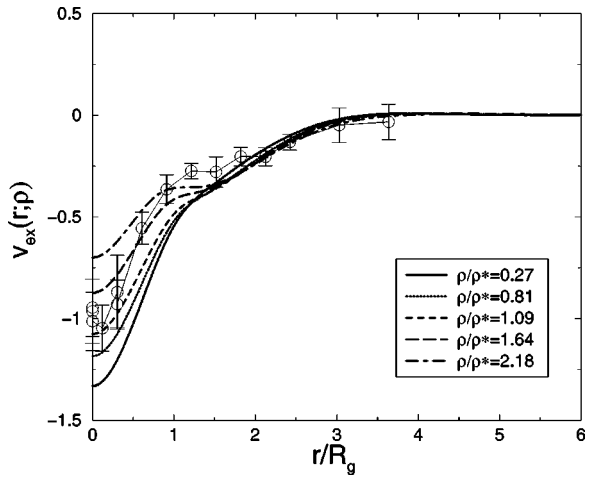

FIG. 5. The density-dependent excess potentials $v_{ex}(r;\rho)$ determined for several densities from the SAW simulations are denoted by the smooth spline fit curves. The open circles with error bars correspond to the evaluation of Eq. (11) at $\rho=0$, the line through them is to guide the eye.

cantly. The difference arises from the neglected many-body interactions, as discussed in Appendix B.

B. Understanding the density dependence of the effective pair potential

Given the success of the density-dependent pair interaction in describing pair correlations and thermodynamics, we next turn to the question of whether the density dependence of $v(r;\rho)$ can be directly understood from the density-independent many-body interactions.

Within the HNC approximation, the following expression due to Reatto and Tau [5] and also Attard [6]

$$v(r_{12};\rho)=w^{(2)}(r_{12})-\rho\int(\exp[-w^{(3)}(r_{12},r_{13},r_{23})]-1)\times g_2(r_{13};\rho)g_2(r_{23};\rho)d\mathbf{r}_3, \quad (10)$$

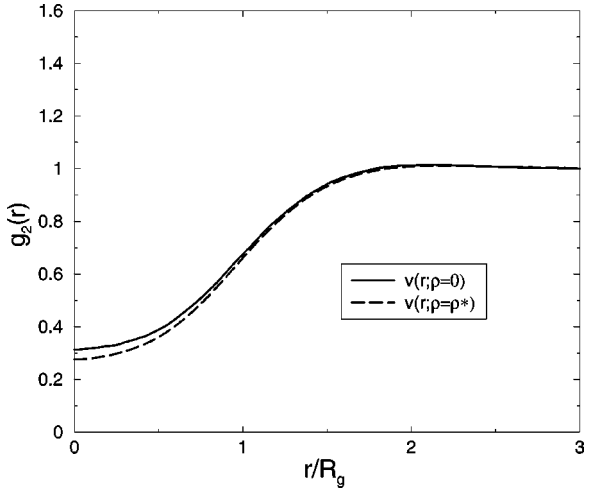

FIG. 4. Comparison of $g_2(r)$'s generated at density $\rho=\rho^*$ by the low-density potential $v(r;\rho=0)$ and the correct potential $v(r;\rho=\rho^*)$. Note how small the differences are.

describes the density dependence of the pair potential that would reproduce the true pair-correlations induced by the two-body and three-body potentials. This is a generalization of earlier expressions [41,42] and neglects terms of order $\mathcal{O}(\rho^2)$ and higher. In the literature it has mainly been applied to the Axilrod-Teller interaction for rare-gas fluids, where it works remarkably well, see, e.g., [43] and references therein.

Figure 5 highlights the density dependence by plotting $v_{ex}(r;\rho)=[v(r;\rho)-w^{(2)}(r)]/\rho$. For clarity, we have replaced the rather noisy data by spline fits. For densities $\rho/\rho^*<1$ the curves are close to each other suggesting that the roughly linear density dependence in Eq. (10) holds true. For larger densities into the semidilute regime, $v_{ex}(r;\rho)$ becomes smaller in magnitude and the density dependence becomes nonlinear. This nonlinearity is not unexpected, since Eq. (10) neglects higher-order terms in ρ, as well as the effects of four-body and higher-order interaction terms.

We can go even further and directly calculate the triplet induced density-dependent term $v_{ex}(r;\rho)$ by substituting Eq (6) into Eq. (10) to obtain

$$v_{ex}(r_{12},\rho)=-\int\left(\lim_{\rho\to 0}\frac{g_3(r_{12},r_{13},r_{23})}{g_2(r_{12})g_2(r_{13})g_2(r_{23})}-1\right)\times g_2(r_{13};\rho)g_2(r_{23};\rho)d\mathbf{r}_3. \quad (11)$$

The $g_2(r;\rho)$, in contrast to the $g_2(r)$ in the first term in Eq. (11), are defined at the density of interest. Evaluating this integral is difficult, because the term between brackets can become very small. We use a direct MC procedure, where two polymer coils are held with their c.m. a distance r_{12} apart while we integrate over the position of the third particle. In order to ensure that the integral converges it is crucial to use the $g_2(r)$ at $\rho=0$ [i.e., those between the brackets in Eq. (11)], from the simulation itself, by calculating it on the fly. This is necessary to avoid small errors in the radial distribution function that build up during the integration over

the volume. The $g_2(r;\rho)$ at finite density are known from previous calculations. The resulting $v_{ex}(r;\rho)$ for $\rho=0$ is plotted in Fig. 5. The results for finite density do not differ by very much.

In conclusion, the density dependence is mainly caused by three-body interactions, at least in the dilute regime. At semidilute densities, higher-order many-body interactions may come into play.

V. MANY-BODY CORRELATIONS

If $g_2(r)$ is generated by a system with only pair potentials, then the exact inversion of $g_2(r)$ at *any* density will reproduce the exact pair potential. For such a system, the inverted pair potential can be used in principle to determine all higher-order correlation functions of the original system. In other words, for systems with only pair interactions, the pair-distribution function $g_2(r)$ contains enough information to generate all higher-order correlation functions [44].

If a system has three-body or higher-order interactions, then our $v(r;\rho)$ still exactly reproduces the pair correlations. But, as we shall demonstrate in this section, it can no longer exactly reproduce the higher-order correlations. Nevertheless, we will show that the differences are not very large for the case of SAW polymers at the densities we study.

A. Bond angle distribution from three-body correlations

Calculating and comparing the full three-body correlation functions would be very cumbersome for many of the same reasons that it is difficult to map out the full three-body interaction. Therefore, we resort to a reduced picture where a subset of the variables are integrated out [45,46]. One popular measure of the three-body interactions is the bond angle distribution function, defined as

$$b(\theta,r_c)=8\pi^2\rho^2N\int_0^{r_c}\int_0^{r_c}g_3(r_{12},r_{13},(r_{12}^2+r_{13}^2 - 2r_{12}r_{13}\cos\theta)^{1/2})r_{12}^2r_{13}^2\sin\theta\, dr_{12}dr_{13}, \tag{12}$$

where N is a dimensionless normalization constant. This integral sums over all triplets within a cutoff radius r_c from the central particle and determines the distribution of the angle θ in these triplets. We calculated the bond angle distribution for both the SAW simulations and the effective pair potentials for different cutoff radii r_c as shown in Fig. 6. The effective potentials $v(r;\rho)$ reproduce this measure of the three-body correlations remarkably well. Since for an ideal gas the bond angle distribution exactly follows a sine curve, dividing the bond angle distribution by $\sin\theta$ highlights the deviations from ideal behavior. In Fig. 7 we show the renormalized bond angle distribution. The differences between the curves are now clearer. The absolute deviations from the sinelike behavior are largest at small θ because the particles repel each other and triplets with small θ will be relatively rare. In the case of a hard sphere systems this correlation hole would be even more pronounced. It is remarkable how

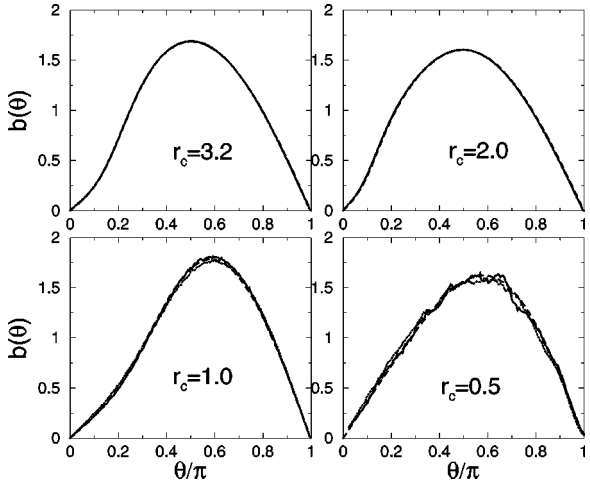

FIG. 6. The bond angle distribution $b(\theta,r_c)$ plotted for several cutoff radii r_c for $\rho=\rho^*$. The solid curves denote the effective potential results, the dotted curves correspond to the explicit SAW simulations and the dashed curves show Kirkwood's superposition approximation.

well the bond order distribution follows the ideal sine curve for the larger angles. At a cutoff radius of $r_c=0.5$ the distribution becomes flatter, reflecting the broad flat top of the repulsive Gaussian shaped pair potential.

Instead of determining the distributions from explicit simulations, we can also substitute the Kirkwood superposition approximation [26]

$$g_3(r_{12},r_{13},r_{23})\approx g_2(r_{12})g_2(r_{13})g_2(r_{23}) \tag{13}$$

into Eq. (12) and calculate the integral directly by using the radial distribution functions from previous simulations. This approximation is also included in Figs. 6 and 7 and turns out to be very accurate, except for $\theta\approx 0$ and $\theta\approx\pi$ (see Fig. 7)

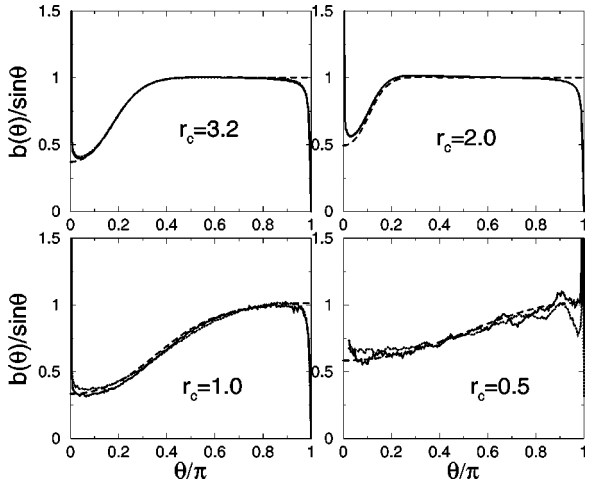

FIG. 7. The normalized bond angle distribution $b(\theta,r_c)$ plotted for several cutoff radii r_c for $\rho=\rho^*$. The solid curves denote the effective potential results, the dotted curves correspond to the explicit SAW simulations, and the dashed curves show Kirkwood's superposition approximation.

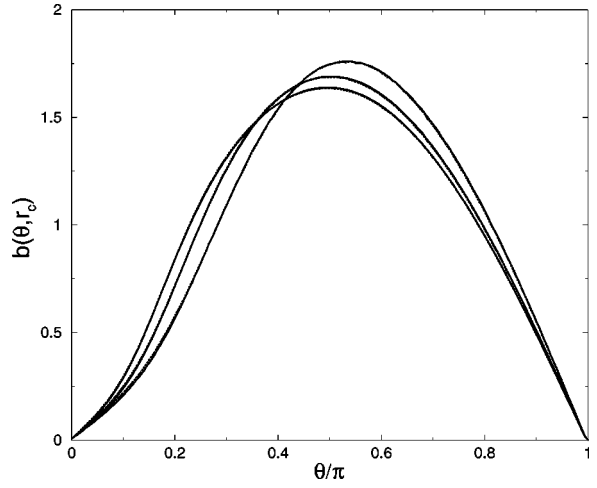

FIG. 8. Comparison between bond angle distribution $b(\theta,r_c)$ for effective potentials $v(r;\rho=0)$ (dotted lines) and $v(r;\rho=\rho^*)$ (solid lines), both determined from simulations at $\rho=\rho^*$. From left to right the curves correspond to $r_c=2.5$ 2.0, and 1.5. The differences are so small that the lines are virtually indistinguishable on the scale of the graph.

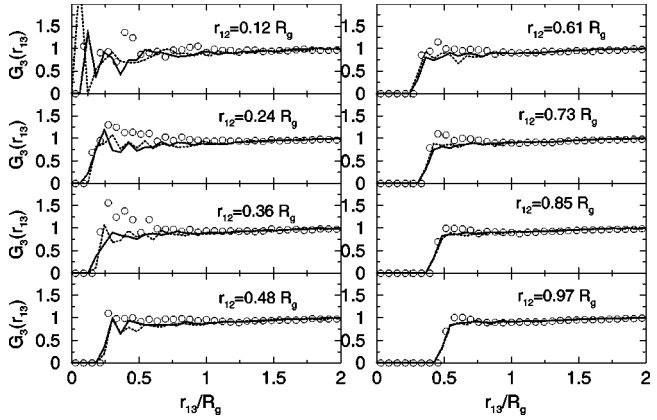

FIG. 9. To measure $G_3(r_{12},r_{13},r_{13})$, which denotes deviations from Kirkwood superposition, we fix r_{12}, and plot the $G_3(r)$ as functions of $r=r_{13}=r_{23}$ (isoceles triangles, see Fig. 1). Results are given for SAW polymers (circles), effective potentials $v(r;\rho)$ (solid lines), and $v(r;\rho=0)$ potentials (dashed lines). All plots are from simulations at $\rho=\rho^*$. Note that the two effective potential plots are more or less identical within the statistical noise, while the SAW $G_3^{SAW}(r)$ is slightly higher by approximately a factor $\exp[-w^{(3)}(r)]$.

where the simulations are prone to large statistical errors, due to the vanishing volume of the available phase-space.

The bond-angle distribution is not very sensitive to differences in the full three-body correlations (see, e.g., Ref. [46]), partially because it is an integrated quantity. An example of this is given in Fig. 8, where the bond angle distributions of the effective potentials $v(r;\rho=0)$ and $v(r;\rho=\rho^*)$ are compared for the same density $\rho=\rho^*$. Clearly, there is hardly any difference between the distributions.

B. Deviations from Kirkwood superposition for three-body correlations

A more sensitive measure of triplet correlations is the deviation from the Kirkwood superposition approximation, Eq. (13), which we define as:

$$G_3(r_{12},r_{13},r_{23})=\frac{g_3(r_{12},r_{13},r_{23})}{g_2(r_{12})g_2(r_{13})g_2(r_{23})}. \qquad (14)$$

Since our $v(r;\rho)$ exactly reproduces the $g_2(r)$, this expression should highlight any differences between the true g_3 and the g_3 arising from our effective potential picture. To simplify, we limit ourselves for a given r_{12} to triplet configurations for which $r=r_{23}=r_{13}$ (i.e., isoceles triangles).

First, we compare in Fig 9 the $G_3(r)$ at $\rho=\rho^*$ generated by $v(r;\rho=0)$ and by $v(r;\rho=\rho^*)$. Just as we found for the bond angle distributions, the $G_3(r)$ are very similar even though the potentials are different. We already showed that the $g_2(r)$ are not very different either (see Fig. 4) , so that the same now holds for the full $g_3(r_{12},r_{23},r_{13})$.

Next, we turn to a comparison between the true $G_3^{\rm SAW}(r)$ derived from explicit simulations of our SAW polymer system and the $G_3^{\rm eff}(r)$ of the effective potentials at $\rho=\rho^*$. As can be seen in Fig. 9, our effective pair-potential $v(r;\rho)$ does not exactly reproduce the SAW three-body correlation function. The trends are similar, but the deviation from superposition of the SAW polymers, $G_3^{\rm SAW}(r)$, is consistently larger than the same quantity generated by the effective potentials $G_3^{\rm eff}(r)$, especially if $r<R_g$.

For systems with an explicit three-body interaction the Kirkwood superposition approximation is sometimes written as

$$g_3(r_{12},r_{13},r_{23})\approx g_2(r_{12})g_2(r_{13})g_2(r_{23}) \times\exp[-w^{(3)}(r_{12},r_{13},r_{23})]. \qquad (15)$$

This is exact in the $\rho\to 0$ limit, as can be seen from Eq. (6). Note that in the same limit the three-body correlations induced by the $v(r;\rho)$ reduce to the simpler Kirkwood superposition approximation $g_3(r_{12},r_{13},r_{23})\approx g_2(r_{12})g_2(r_{13})g_2(r_{23})$, demonstrating explicitly that in contrast to the two-body correlations, $v(r;\rho)$ cannot exactly reproduce the three-body correlations if there is a three-body interaction present. In fact, we have shown explicitly that two systems with identical pair correlations, namely, our effective potential system and the original SAW system, can have differing triplet correlations.

These arguments also suggest that a simple approximation, namely $G_3^{SAW}(r)\approx G_3^{\rm eff}(r)\exp[-w^{(3)}(r)]$, can shed some light on the differences observed in Fig. 9. Since $w^{(3)}(r)$ is negative for equilateral triangle configurations, as illustrated in Fig 2, it is perhaps not surprising that roughly speaking $G_3^{SAW}(r)>G_3^{eff}(r)$ for the isoceles triangle configurations plotted in Figs 9, at least in the region where $w^{(3)}(r)$ is nonzero. Unfortunately the statistical errors in this region are very large, making a quantitative comparison difficult, but the deviation is certainly of the same order as would be expected from an extra factor $\exp[-w^{(3)}(r)]$ (compare with Fig. 2).

Our very simple approximation illustrates how deviations from Kirkwood superposition originate from two effects:

(1) Deviations induced by correlations generated by the pair-potentials alone. These have been studied in great detail for hard-sphere systems, see, e.g., Refs. [47,48].

(2) Deviations induced primarily by three-body potentials.

In practice, of course, these two effects are somewhat entwined, especially at higher densities. Nevertheless, splitting the two effects can shed light on the origin of three-body correlations. In particular, it suggests that while an effective pair potential $v(r;\rho)$ that exactly reproduces the $g_2(r)$ can partially reproduce deviations from superposition of type (1), it will fail for deviations of type (2).

Since the three-body and higher-order interactions between the c.m.'s of polymer solutions are not very strong, the total $g_3(r)$'s are still remarkably well reproduced by the $v(r;\rho)$, especially when integrated quantities such as the bond-angle correlations are considered. However, for systems where three-body interactions are strong, such as liquid Si or liquid Ga, one cannot expect the same success from effective pair potentials. Very similar conclusions were stressed by Evans [44] in the context of reverse Monte Carlo simulations [46,49].

VI. CONCLUSIONS

Integrating out the monomeric degrees of freedom to obtain a description based on effective potentials between polymer c.m.'s is a useful coarse-graining technique for polymer solutions. Because simulations can be performed to high accuracy, the lessons learned here should be relevant to a much broader range of coarse-graining schemes.

In particular, we showed that the free energy of the polymers can be expanded in a series of state-independent many-body effective potentials. At full overlap the terms in the series oscillate in sign as $(-1)^n$, and become smaller in absolute magnitude for increasing n. The scaling theory developed in Appendix A confirms these ideas, and can be used to extend them to arbitrary order n.

A parallel description of the coarse-grained polymer solution was developed in terms of an effective state (density) dependent pair potential $v(r;\rho)$, which exactly reproduces the pair-correlations and, in an average way, includes all the higher-order terms in the many-body free energy expansion. The density-dependence of this effective pair potential can be largely understood from the direct influence of the density-independent three-body interactions.

The three-body correlations are also well described by this effective pair-potential picture. If the bond angle distribution is used, the differences between the full SAW polymer system and our effective pair-potential picture are almost indistinguishable. However, this is not a good ''order parameter'' for measuring deviations in three-body distribution functions, since there is almost no difference between results from the full simulations and those produced with the Kirkwood superposition approximation. When we use a more direct measure of the deviations from Kirkwood superposition, small differences between the effective two-body and the full SAW triplet distributions can be measured. These arise primarily from the direct effect of the three-body potential $w^{(3)}(r)$, and illustrate a more general point, namely, that an effective two-body interaction can never simultaneously reproduce the two and three-body correlations in a system with many-body interactions exactly. Since for polymers in a good solvent these many-body interactions are relatively weak, a coarse-grained description based on effective pair interactions works remarkably well, at least for the dilute and the beginning of the semidilute regime [23,24]. Whether this success can be extended deeper into the semidilute or into the melt regime, or even for polymers in poor solvents, remains to be seen, and will be the subject of future investigations.

ACKNOWLEDGMENTS

A.A.L. acknowledges support from the Isaac Newton Trust, Cambridge. P.B. acknowledges support from the EPSRC under Grant No. GR/M88839. We thank H. Löwen and C. von Ferber for useful discussions, and R. Finken and V. Krakoviak for a critical reading of the manuscript.

APPENDIX A: RELATIVE STRENGTH OF *n* BODY TERMS FROM SCALING THEORY

In a recent paper, von Ferber *et al.* [25] used scaling theory and simulations to calculate the triplet interaction for star-polymers and found an attractive interaction with a relative strength of about 11%, very similar to our three-body results. The natural choice for the position coordinate of a star polymer is not the c.m., but its midpoint [50]. However, we will see that for estimating relative contributions, the difference between our c.m. representation and the midpoint representation is not too important.

Here, we apply the star polymer scaling theory to estimate the relative contributions of $w^n(0)$ to all orders in n. We specialize to linear polymers, which can be seen as star-polymers with only two arms. We first note that the partition function for n polymers with their mid points constrained to be a distance $r \ll R_g$ apart scales as [25,51,52]

$$Z_n(r) \sim r^{\theta_n}, \tag{A1}$$

in the limit $r/R_g \to 0$. Here θ_n is the contact exponent, which in turn can be written as

$$\theta_n = n\,\eta_2 - \eta_{2\cdot n}, \tag{A2}$$

where the η_f are the scaling exponents for a star polymer with f arms. These are tabulated for two different renormalization group calculations in [25,53], and can also be approximated by a simpler expression

$$\eta_f \approx 0.3353 f^{3/2}, \tag{A3}$$

which is expected to become more accurate for larger f [54]. Comparing the different approximations gives an indication of the accuracy of the scaling theory results.

The probability of finding n polymers with their midpoints a distance $r \ll R_g$ apart can be found from the partition functions since

TABLE I. Comparison of scaling theory and simulations for many-body interactions between the polymer c.m. The labels a and b denote results that follow from two different renormalization group calculations for the exponents η_n [25], while label c comes from the simple expansion of Eq. (A3), and label d denotes simulation results for $L=500$ SAW polymer simulations.

n	2	3	4	5	6	7	8	9	10
a θ_n/θ_2	$1(\theta_2=0.8)$	2.55	4.49	6.75	9.3				
b	$1(\theta_2=0.82)$	2.65	4.80	7.41	10.43				
c	$1(\theta_2=0.79)$	2.65	4.83	7.46	10.50	13.90	17.66	21.73	26.10
d $\ln g_n(0)/\ln g_2(0)$	$1(\ln g_2(0)=1.88)$	2.74 ± 0.01	5.13 ± 0.02	7.99 ± 0.05					
a $\hat{w}^{(n)}/\hat{w}^{(2)}$	$1(\hat{w}^{(2)}=0.8)$	-0.45	0.29	-0.19	0.11				
b	$1(\hat{w}^{(2)}=0.82)$	-0.35	0.22	-0.15	0.085				
c	$1(\hat{w}^{(2)}=0.79)$	-0.35	0.22	-0.17	0.14	-0.12	0.11	-0.10	0.094
d $w^{(n)}(0)/w^{(2)}(0)$	$1(w^{(2)}(0)=1.88)$	-0.26 ± 0.013	0.17 ± 0.031	-0.21 ± 0.08					
a $\Delta w^n(0)$		-0.15	0.069	-0.027	0.012				
b		-0.12	0.048	-0.019	0.0083				
c		$-0.12??$	0.049	-0.023	0.014	-0.0088	0.0063	-0.0046	0.0036
d		-0.09 ± 0.004	0.034 ± 0.007	-0.026 ± 0.01					

$$-\lim_{\rho\to 0}\ln g_n^{mid}(r)\propto \ln[Z_n(r)]\sim \theta_n \ln(r/R_g). \tag{A4}$$

Here $g_n^{mid}(r)$ is the n-body distribution function for the midpoints of n polymers. These scaling theories can be developed for polymers in the midpoint representation in part because of the analogy of the overlap of n polymers to a $2n$ arm star polymer. Such an analogy is not as obvious for the c.m. representation, hampering the derivation of a c.m.-based scaling theory. On the other hand, MC simulations for overlap in the c.m. representation are much easier than for the midpoint representation because the probability $g_n(r)$ is much larger than $g_n^{mid}(r)$ in the small r limit, in fact $g_n^{mid}(0)=0$ while the c.m. $g_n(0)$ is finite. Gathering good statistics for the mid-point representation is thus much slower than for the c.m. representation. It, nevertheless, seems reasonable to expect that the *relative* strengths of different orders of the interactions in the c.m. representation are similar to those of the midpoint representation, suggesting that the relative probability of full overlap of the c.m. of n polymers scales as

$$\lim_{\rho\to 0}\left(\frac{\ln g_n(0)}{\ln g_m(0)}\right)\approx \lim_{r\to 0}\lim_{\rho\to 0}\left(\frac{\ln g_n^{mid}(r)}{\ln g_m^{mid}(r)}\right)\approx\frac{\theta_n}{\theta_m}. \tag{A5}$$

In Table I we confirm this ansatz by comparing $\ln g_n(0)/\ln g_2(0)$ calculated by direct simulations for $n=3,4,5$ with θ_n/θ_2 calculated by three different versions of the scaling theory. Clearly, all three scaling theories and the simulations agree reasonably well with each other, giving us confidence to proceed.

Armed with this approximate equivalence of the g_n's in the two representations, we can now fruitfully compare the strength of the n-body interaction $w^{(n)}(0)$ for c.m. particles to an expression derived from the scaling theory, by using Eqs. (A2) and (A4) to recursively rewrite Eq. (9) as

$$w^{(n)}(0)\propto\hat{w}^{(n)}=(-1)^n\sum_{m=2}^{n}\binom{n}{m}(-1)^m(m\eta_2-\eta_{2\cdot m}). \tag{A6}$$

Here $\hat{w}^{(n)}$ is the coefficient of the full (divergent) midpoint-midpoint interaction, $w_{mid}^{(n)}(r)\sim\hat{w}^{(n)}\ln(r/R_g)$ in the limit $r\to 0$. The values of these terms relative to the $n=2$ term are compared in Table I with direct simulation results for $n=3,4,5$, and again good agreement is obtained. For the scaling theory each higher-order term is opposite in sign and smaller than the previous one. Our simulations show the same trend for the sign, but the error bars on the $n=5$ simulations are still too large to ascertain that its magnitude is less than the $n=4$ term.

The strength of the n-body term contribution to the free energy relative to all lower-order terms can also be found from the arguments above. In this case the prefactors cancel and we find

$$\Delta w^{(n)}(0)\approx\Delta\hat{w}^{(n)}=\frac{\hat{w}^{(n)}}{\theta_n-\hat{w}^{(n)}}. \tag{A7}$$

Once again the simulations and the scaling theory agree quite well both for the magnitude and the sign of the different terms.

APPENDIX B: CONVERGENCE OF THE FULL FREE ENERGY SERIES

The good agreement found between the scaling theory and the simulations for $n=3,4,5$ suggests that we can evaluate trends for arbitrary order n from the scaling theory. We use the simple expression in Eq. (A3) that gives η_f for arbitrary f, to simplify Eq. (A6) to

$$\hat{w}^{(n)}=0.9484(-1)^n\left[\sum_{m=1}^{n}\binom{n}{m}(-1)^{m+1}m^{3/2}\right]. \tag{B1}$$

The sum between brackets is positive for all n, and becomes smaller for each subsequent term. For example, for $n=3$ it is 0.29, while for $n=10\,000$, it is has dropped to 0.009. This implies that at all orders, the n-body interaction $w^{(n)}(0)$ oscillates in sign as $(-1)^n$ and decreases in absolute magnitude with increasing n. The absolute magnitudes of the relative contributions $\Delta w^{(n)}(0)$ decrease even faster with n.

We expect that the absolute magnitude of each n-body term is largest at full overlap. However, the fact that each higher-order term decreases in absolute magnitude, or even that the terms oscillate in sign at $r=0$, does not necessarily imply that the full free energy expansion of Eq. (1) will converge quickly for all configurations $\{\mathbf{r}_i\}$ of the c.m. For one thing, for an N particle system, the number of n-tuple coordinates grows as the binomial $N!/(N-n)!n!$. Therefore, even though the magnitude of the n-body terms $w^{(n)}(\mathbf{r}_{i_1},\mathbf{r}_{i_2},\ldots,\mathbf{r}_{i_n})$ becomes smaller with increasing n, the number of such terms at each order n in the free energy series Eq. (1) increases almost exponentially with increasing n. Of course for a given configuration $\{\mathbf{r}_i\}$, not only the magnitude, but also the range of each term $w^{(n)}(\mathbf{r}_{i_1},\mathbf{r}_{i_2},\ldots,\mathbf{r}_{i_n})$ is needed to decide how many, if not all N terms, are needed to calculate the full free energy to a desired accuracy. As mentioned before, calculating the complete dependence of $w^{(n)}(\mathbf{r}_{i_1},\mathbf{r}_{i_2},\ldots,\mathbf{r}_{i_n})$ on all possible n-tuple c.m. coordinates $\{\mathbf{r}_{i_1},\mathbf{r}_{i_2},\ldots,\mathbf{r}_{i_n}\}$ is usually an impossible task for higher-order n.

Nevertheless, some progress can be made by looking at the special case of a set $\{\mathbf{r}_i\}$ where all N c.m.'s are at the same point. This is simply the situation studied in the previous section by scaling theory, for which the free energy is given by

$$\mathcal{F}(N,V,\{\mathbf{r}_i\})-\mathcal{F}^{(0)}(N,V)=-\ln g^N(0)\propto\theta_N. \qquad \text{(B2)}$$

Ignoring for the moment the volume term, who's contribution is expected to be negligible [17,24], we can ask the question: How well is the free energy described by taking only pair-interaction terms into account? Since there are $\frac{1}{2}N(N-1)$ pair terms, the free energy with only pair terms taken into account scales as $\mathcal{F}\propto N(N-1)w^{(2)}(0)\sim N^2$ while the true free energy scales as $\mathcal{F}\propto\theta_N\sim N^{3/2}$. Including only the pair terms heavily *overestimates* the free energy, a result also found by von Ferber *et al.* [25]. In other words, if one truncates the coarse-grained free energy series in Eq. (1) then certain configurations $\{\mathbf{r}_i\}$ will not be properly accounted for.

However, if one were to use this coarse-grained free energy series to study a given polymer solution, then the relative probability for finding a configuration at complete overlap of the c.m. would be very small. On the other hand, for any given order n, the probability of finding n-fold overlap increases with increasing density, so that one would expect to need more and more terms in the coarse-grained free energy series as the density increases.

Another way to measure the effects of truncating the coarse-grained free energy series in Eq. (1) would be to compare it to the excess free energy per particle for the original polymer solution. This can be found by averaging $\mathcal{F}(N,V,\{\mathbf{r}_i\})$ over all configurations $\{\mathbf{r}_i\}$ to obtain the total free energy $F(N,V)$, as done in Eq. (2). Including only pair interactions in our c.m. representation of polymer solutions casts the problem into that of finding the free energy of a mean-field fluid [33,39,40] for which the excess free energy per polymer scales as

$$\frac{F^{ex}}{N}\sim\rho, \qquad \text{(B3)}$$

while the true excess free energy of a polymer solution in the semidilute regime follows from scaling theory [28]

$$\frac{F^{ex}}{N}\sim\rho^{1/(3\nu-1)}\approx\rho^{1.3}. \qquad \text{(B4)}$$

Whereas including only the pair interactions in an average over all configurations $\{\mathbf{r}_i\}$ in the semidilute regime *underestimates* the total free energy, taking into account only pair terms for single configuration $\{\mathbf{r}_i\}$ at complete overlap of the c.m. *overestimates* the coarse-grained free energy. This implies that the special configurations where the coarse-grained free energy series in Eq. (1) breaks down do not have a strong influence on the thermodynamics.

[1] R. Car and M. Parrinello, Phys. Rev. Lett. **55**, 2471 (1985).
[2] B.M. Axilrod and E. Teller, J. Chem. Phys. **11**, 299 (1943).
[3] J.A. Barker, Mol. Phys. **80**, 815 (1993).
[4] D. Levesque, J.J. Weis, and J. Vermesse, Phys. Rev. A **37**, 918 (1988); D. Levesque and J.J. Weis, *ibid.* **37**, 3967 (1988).
[5] L. Reatto and M. Tau, J. Chem. Phys. **86**, 6474 (1987).
[6] P. Attard, Phys. Rev. A **45**, 3659 (1991).
[7] N.W. Ashcroft and D. Stroud, Solid State Phys. **33**, 1 (1978).
[8] A.E. Carlsson, Solid State Phys. **43**, 1 (1990).
[9] A.A. Louis and N.W. Ashcroft, Phys. Rev. Lett. **81**, 4456 (1998); J. Non-Cryst. Solids **250-252**, 9 (1999).
[10] M. Pearson, E. Smargiassi, and P.A. Madden, J. Phys.: Condens. Matter **5**, 3221 (1993).
[11] J.P. Hansen and H. Löwen, Annu. Rev. Phys. Chem. **51**, 209 (2000).
[12] H. Löwen and E. Allahyarov, J. Phys.: Condens. Matter **10**, 4147 (1998).
[13] M.J. Grimson and M. Silbert, Mol. Phys. **84**, 397 (1991).
[14] R. van Roij and J.P. Hansen, Phys. Rev. Lett. **79**, 3082 (1997); H. Graf and H. Löwen, Phys. Rev. E **57**, 5744 (1998); R. van Roij, M. Dijkstra and J.P. Hansen, *ibid.* **59**, 2010 (1999).
[15] R. van Roij and R. Evans, J. Phys.: Condens. Matter **11**, 10 047 (1999); P.B. Warren, J. Chem. Phys. **112**, 4683 (2000).
[16] M. Dijkstra, R. van Roij, and R. Evans, Phys. Rev. E **59**, 5744 (1999).
[17] C.N. Likos, Phys. Rep. **348/4-5**, 267 (2001).
[18] S. Melchionna and J.P. Hansen, Phys. Chem. Chem. Phys. **2**, 3465 (2000); D. Goulding and S. Melchionna, *ibid.* (to be pub-

lished).
[19] P.J. Flory and W.R. Krigbaum, J. Chem. Phys. **18**, 1086 (1950).
[20] A.Y. Grosberg, P.G. Khalatur, and A.R. Khokhlov, Makromol. Chem., Rapid Commun. **3**, 709 (1982).
[21] J. Dautenhahn and Carol K. Hall, Macromolecules **27**, 5399 (1994).
[22] B. Krüger, L. Schäfer, and A. Baumgärtner, J. Phys. (France) **50**, 319 (1989).
[23] A.A. Louis, P.G. Bolhuis, J.P. Hansen, and E.J. Meijer, Phys. Rev. Lett. **85**, 2522 (2000).
[24] P.G. Bolhuis, A.A. Louis, E.J. Meijer, and J-P Hansen, J. Chem. Phys. **114**, 4296 (2001).
[25] C. von Ferber, A. Jusufi, C.N. Likos, H. Löwen, and M. Watzlawek, Eur. Phys. J. E **2**, 311 (2000).
[26] J.G. Kirkwood, J. Chem. Phys. **20**, 929 (1952).
[27] P.J. Flory, *Principles of Polymer Chemistry* (Cornell University Press, Ithaca, NY, 1953).
[28] P.G. de Gennes, *Scaling Concepts in Polymer Physics* (Cornell University Press, Ithaca, NY, 1979).
[29] M. Doi, *Introduction to Polymer Physics* (Oxford University Press, Oxford, 1995).
[30] N. Madras and A.D. Sokal, J. Stat. Phys. **50**, 109 (1988).
[31] D. Frenkel and B. Smit, *Understanding Molecular Simulations* (Academic Press, New York, 1995).
[32] M. Dijkstra, D. Frenkel, and J.P. Hansen, J. Chem. Phys. **101**, 3179 (1994).
[33] A.A. Louis, e-print cond-mat/010220; Philos. Trans. R. Soc. London, Ser. **359**, 939 (2001).
[34] R.L. Henderson, Phys. Lett. **49A**, 197 (1974); J.T. Chayes and L. Chayes, J. Stat. Phys. **36**, 471 (1984).
[35] L. Reatto, Philos. Mag. A **58**, 37 (1986); L. Reatto, D. Levesque, and J.J. Weis, Phys. Rev. A **33**, 3451 (1986).
[36] J.P. Hansen and I.R. McDonald, *Theory of Simple Liquids*, 2nd ed. (Academic Press, London, 1986).
[37] P.G. Bolhuis and A.A. Louis (unpublished).
[38] Note, however, that this does not include the role of possible volume terms [14] which are independent of pair correlations. Here we expect the volume term contribution to be very small [17], as evidenced by the fact that our effective potentials accurately reproduce the total polymer equation of state [24]. See also [33] and references therein. Even without volume terms, obtaining the correct thermodynamics from a density dependent pair potential can be subtle [see, e.g., M.A. van der Hoef and P.A. Madden, J. Chem. Phys. **111**, 1520 (1999)]. The compressibility route follows from properties of the distribution functions and is independent of the underlying interactions, but the virial route cannot always be trusted [A.A. Louis (to be published)].
[39] A.A. Louis, P. Bolhuis, and J.P. Hansen, Phys. Rev. E **62**, 7961 (2000).
[40] C.N. Likos, A. Lang, M. Watzlawek, and H. Löwen, Phys. Rev. E **63**, 031206 (2001).
[41] J.S. Rowlinson, Mol. Phys. **52**, 567 (1984).
[42] G.S. Rushbrooke and M. Silbert, Mol. Phys. **12**, 505 (1967).
[43] J.A. Anta, E. Lomba, and M. Lombardero, Phys. Rev. E **55**, 2707 (1997).
[44] R. Evans, Mol. Simul. **4**, 409 (1990).
[45] H. Lowen and G. Kramposthuber, Europhys. Lett. **23**, 637 (1993).
[46] F.L.B. da Silva, B. Svensson, T. Åkesson, and B. Jönsson, J. Chem. Phys. **109**, 2624 (1998).
[47] J.L. Barrat, J.P. Hansen, and G. Pastore, Mol. Phys. **63**, 747 (1988).
[48] A. Khein and N.W. Ashcroft, Phys. Rev. E **59**, 1803 (1999).
[49] R.L. McGreevey and M.A. Howe, Annu. Rev. Mater. Sci. **22**, 217 (1992); L. Pusztai and G. Tóth, J. Chem. Phys. **94**, 3042 (1991).
[50] C.N. Likos *et al.*, Phys. Rev. Lett. **89**, 4450 (1998); M. Watzlawek, C.N. Likos, and H. Löwen, *ibid.* **82**, 5289 (1999).
[51] B. Duplantier, J. Stat. Phys. **54**, 581 (1989).
[52] C. von Ferber, Nucl. Phys. B **490**, 511 (1997).
[53] C. von Ferber and Y. Holovatch, Phys. Rev. E **56**, 6370 (1997).
[54] K. Ohno, Phys. Rev. A **40**, 1524 (1989).